Canadian Science Publishing | Botany

Coastal picocyanobacteria can exploit low oxygen habitats

Journal:	*Botany*
Manuscript ID	Draft
Manuscript Type:	Research Article
Date Submitted by the Author:	n/a
Complete List of Authors:	Śliwińska-Wilczewska, Sylwia; Mount Allison University, Department of Biology; University of Gdansk, Institute of Oceanography Savoie, Mireille ; Mount Allison University, Department of Biology Campbell, Douglas ; Mount Allison University, Department of Biology
Is the manuscript for consideration in a Special Issue or Collection?:	Plant community and diversity for the UN Decade on Ecosystem Restoration
Keyword:	Colour, niches, OMZs, oxygen concentration, PC-rich strain, PE-rich strain, spectral wavebands, Synechococcus

Coastal picocyanobacteria can exploit low oxygen habitats

Sylwia Śliwińska-Wilczewska[1,2], Mireille Savoie[1], and Douglas A. Campbell[1,✉]

[1] Department of Biology, Mount Allison University, 53 York St., Sackville, NB, E4L 1C9, Canada

[2] Institute of Oceanography, University of Gdansk, 46 Pilsudskiego St, P81-378, Gdynia, Poland

✉ Correspondence: Douglas A. Campbell: dubhglascambeuil@gmail.com

Abstract

The picocyanobacterial genus *Synechococcus*, one of the most abundant primary producers in marine ecosystems, comprises a diversity of strains of differing pigmentations, thriving across diverse niches. Oxygen Minimum Zones with low [O_2] are expanding in both open ocean and coastal habitats. We found that PhycoCyanin- and PhycoErythrin-rich *Synechococcus* both grow under 2.5 µM [O_2], characteristic of Oxygen Minimum Zones, across a range of spectral wavebands from 405 – 730 nm. The PhycoCyanin-rich strain showed generally similar chlorophyll-specific growth rates (µ; d^{-1}) under 2.5 and 250 µM [O_2], whereas PhycoErythrin-rich cultures achieved faster growth rates, across the spectral bandwidths, under 2.5 µM [O_2] than under 250 µM [O_2]. For PhycoCyanin- and PhycoErythrin-rich *Synechococcus*, µ showed also positive linear responses to both Phycobiliproteins:Chlorophyll *a*, and to cumulative diel PSII electron flux, although the relations vary across strain and [O_2]. Electron transport downstream of Photosystem II was generally higher for both PhycoCyanin- and PhycoErythrin-rich strains under 250 µM [O_2], since cyanobacteria show strong capacity for electron flow away from PSII to O_2, particularly

under excess excitation. In spite of this stronger electron transport under 250 µM [O_2], the PhycoErythrin-rich strain showed a higher growth yield of electron transport under 2.5 µM [O_2]. PhycoErythrin-rich *Synechococcus* are currently typically found at greater depths, and lower light, than are PhycoCyanin-rich strains, but we suggest that the PhycoErythrin-rich strains are actually limited to lower light by an interaction between light and full air-saturated [O_2]. In expanding Oxygen Minimum Zones PhycoErythrin-rich strains will likely exploit higher light niches, across a wider spectral range.

Key words: Colour, niches, OMZs, oxygen concentration, PC-rich strain, PE-rich strain, spectral wavebands, *Synechococcus*

Introduction

Since the mid-20th century, declining oxygen concentrations in regions of the open ocean, and in coastal waters (Breitburg et al. 2018) are affecting productivity, biodiversity, and biogeochemical cycles in marine ecosystems (Keeling et al. 2010). Low oxygen environments in the ocean, termed Oxygen Minimum Zones (OMZ) have expanded to an area equivalent to the European Union, and the global volume of oxygen-free water has quadrupled (Breitburg et al. 2018). It is thus necessary to understand which species will survive and dominate under ongoing and predicted changes in ocean and coastal oxygen concentrations.

Oxygenic picocyanobacteria numerically dominate the phytoplankton across vast tracts of the world's oceans, notably in oligotrophic regions, but also in some coastal ecosystems (Larsson et al. 2014; Śliwińska-Wilczewska et al. 2018a; Aguilera et al. 2023). Oxygen is a product of photosynthesis, and a substrate for reductant consumption, but also has potential to damage

Photosystem II (PSII) protein subunits (Andersson et al. 1992). The oxygen evolving complex of PSII can also be directly inactivated by a photon in the UV or blue range directly absorbed by the Mn_4Ca cluster (Hakala et al. 2005; Partensky et al. 2018); therefore, oxygen interacts with spectral band to influence the balance between productive photosynthesis and costly photoinactivations (Murphy et al. 2017). OMZ pose challenges for aerobic organisms (Breitburg et al. 2018), but picocyanobacteria inhabiting OMZs have genetic adaptations enabling them to tolerate and even thrive in oxygen-depleted environments, such as changes in energy metabolism, antioxidant defense mechanisms, and cellular structures optimized for oxygen scavenging and storage (Ulloa et al. 2012, 2021; Bagby and Chisholm 2015; Partensky et al. 2018; Callieri et al. 2022; Wong et al. 2023).

Picocyanobacteria also show photosynthetic adaptations to spectral wavebands, ranging from short-wavelength blue light (Luimstra et al. 2018), through green and yellow light to long-wavelength red light. Plankton ecologists have long acknowledged that a diverse array of photosynthetic pigments allows cyanobacteria species to exploit different spectral wavebands (Falkowski et al. 2004; Stomp et al. 2007). The ecological success of picoplanktonic *Synechococcus* strains throughout the photic oceanic water column (Flombaum et al. 2013) results in part from diverse strategies to respond to variations in their environment (Scanlan 2012). The genus *Synechococcus* is genetically diverse and divided into several major clusters. Picocyanobacteria from *Synechococcus* cluster 5, often found in marine, brackish and freshwater environments (Aguilera et al. 2023), includes sub-clusters of strains rich in phycoerythrin (PE-rich), which imparts a range of orange, reddish, pink, and purple colors, as well as sub-clusters of strains rich in phycocyanin (PC-rich), which color the organism in various shades of blue-green

(Stomp et al. 2004). Competition experiments demonstrate that PC-rich and PE-rich strains can coexist in white light but show spectral niche differentiation (Haverkamp 2008).

PE-rich strains, with high content of the chromophore phycourobilin (PUB), dominate oligotrophic deep waters where blue light predominates, and deep communities in more mesotrophic marine waters, characterized by blue-green light environments (Stomp et al. 2004; Haverkamp et al. 2009) are shifting towards PE-rich Synechococcus with more phycoerythrobilin (PEB). Conversely, PC-rich strains prevail near the surface, and in turbid waters where orange and red light dominate. The widespread coexistence of PC-rich and PE-rich picocyanobacteria is observed in waters of intermediate turbidity, such as mesotrophic lakes and coastal seas (Haverkamp 2008; Haverkamp et al. 2009).

Our aim was to test the growth and functional responses of PC-rich and PE-rich *Synechococcus* cultures to the interaction of different oxygen concentrations (250 µM or 2.5 µM [O_2]), and spectral wavebands (405 – 730 nm). We thus empirically answer the question posed by Wong et al. (2023) regarding the sensitivity of modern picocyanobacteria to low levels of O_2 and a wide range of wavebands found across depths and trophic levels.

Materials and methods

Culture condition and experimental setup

Xenic cultures of PC-rich (CCBA_077) and PE-rich (CCBA_127) *Synechococcus* were obtained from the Culture Collection of Baltic Algae (https://ccba.ug.edu.pl/pages/en/home.php) (Latala et al. 2006). *Synechococcus* strains were cultured in Tissue Culture Flasks (VWR International, Cat. No. 10062-872, PA, USA) and transferred biweekly to fresh f/2 media (Guillard 1975) prepared at a salinity of 8 PSU, reflective of their natural brackish habitat. Pre-cultures were

maintained in incubators with full air saturated dissolved oxygen concentration [O_2] of 250 µM, 22℃, with a light/dark cycle of 12 hours (h) and Photosynthetically Active Radiation (PAR) of 10 µmol photons $m^{-2}s^{-1}$ from Philips Cool White F14T5/841 Alto, 14 watts, fluorescent bulbs.

Controlled growth experiments were performed using MCMIX-OD PSI Multicultivators (Photon Systems Instruments, Drásov, Czech Republic) set to 22℃. Each of 8 round bottom cylindrical glass tubes contained 75 mL of f/2 medium and 5 mL of growing pre-culture. These parameters allowed for exponential growth of the cultures from the beginning of the experiment, with little lag phase. Inoculation of culture tubes took place in the afternoon, with a period of low light and then 12 h darkness before a sinusoidal 12 h photoperiod cycle commenced at 07:00 the following morning, with peak PAR of 180 µmol photons $m^{-2}s^{-1}$ reached at 13:00 each day.

Each tube was maintained under an individual combination of one of 7 spectral wavebands centred at 405, 450, 470, 530, 620, 660, or 730 nm and under 250 µM or 2.5 µM [O_2]. Culture tubes were closed with a silicone inert silicone stopper perforated by an aeration input tube extending to the bottom of the culture tube, and a pressure outlet tube. We used aeration with a total gas flow rate of around ~ 140 mL min^{-1} $tube^{-1}$ through a 0.2µm sterile microfilter provided via a G400 gas mixing system (Qubit Systems Inc., Kingston, Ontario, Canada). ~ 250 µM [O_2] was achieved by sparging with lab air (78% N_2, 21% O_2, 1% Ar and 0.05% CO_2). ~ 2.5 µM [O_2] was achieved by sparging with a gas mixture containing 99.95% N_2 and 0.05% CO_2. [O_2] *in situ* was verified using oxygen optodes (PyroScience, Germany) inserted into tubes for real-time measurements (data not presented), with software correction to account for the salinity of the media (8 PSU). The pH of tested cultures remained about 8, with limited fluctuation during the growth experiment (data not presented).

Chlorophyll-specific growth rates

Picocyanobacterial growth was monitored every 5 minutes by automatically recording OD_{680}, OD_{720}, and ΔOD (ΔOD = OD_{680} – OD_{720}) for at least 5 days, independently for each culture tube. The chlorophyll-specific growth rates (μ) were determined by fitting logistic growth curves using a modified Levenberg-Marquardt fitting algorithm (Elzhov et al. 2023) to plots of the chlorophyll *a* proxy of ΔOD vs. elapsed time (d) for each combination of strain, spectral waveband, and [O_2].

Picocyanobacteria cell counts

Picocyanobacterial cells mL^{-1} were estimated using linear regression models of OD at 680 nm or 720 nm vs. calibration counts of cell suspension densities (cell mL^{-1}) (Table S1). The OD of cultures was measured using MCMIX-OD PSI Multicultivators (Photon Systems Instruments, Drásov, Czech Republic) and cell suspension density measures were conducted using an ImageXpress Pico Digital microscope equipped with CMOS camera and LED+ image autofocus (ImageXpress Pico Automated Cell Imaging System, Molecular Devices, LLC., CA, USA). Culture samples were preserved with 4% glutaraldehyde and kept at -80°C until the microscopy measures. Fixed samples of culture (V = 10 μL) were transferred to surface treated Tissue Culture (TC) black walled 96-well plates (Corning® Falcon® Microplate, MilliporeSigma, Merck, Darmstadt, Germany) with a transparent flat bottom containing 200 μL of f/2 media and centrifuged using a Beckman J-20 centrifuge with a swinging bucket JS-4.3 rotor at 4500 rpm (Beckman Coulter, Brea, California, United States). Cells were imaged with the Cy5 channels (Excitation: 630/40 nm; Emission: 695/45 nm; Dichroic: 655 nm) using selectable confocal geometries, which differentiates cyanobacterial cells from co-occurring heterotrophic bacteria, and

counted using a 63x objective in fluorescence imaging modes. Quantitative analysis on images acquired from automated microscopy obtained from 96-well microplates was performed using the CellReporterXpress Image Acquisition and Analysis Software. The representative cell number mL^{-1} was calculated based on the dilution factor and selected count area from each well (Wlodkowic et al. 2022).

Pigment content and pigment ratio

Whole-cell absorbance spectra of picocyanobacteria cells were collected using an integrating cavity spectrophotometer (CLARiTY 17 UV/Vis/NIR, On-Line Instrument Systems, Inc., Bogart, GA, USA) according to the method proposed by Blake and Griff (2012). The sample and reference observation cavities of the spectrophotometer were filled with 8 mL of f/2 medium at salinity 8 PSU. After establishing a baseline absorbance spectra from 375 to 710 nm, 4 mL culture medium was replaced with 4 mL of culture in the sample cavity. Pathlength corrected absorbance per cm was calculated using Jávorfi coefficients (Jávorfi et al. 2006). We then conducted estimations of pigment content (µg mL^{-1}) including Chlorophyll *a* (Chl *a*), Carotenoids (Car), Phycoerythrin (PE), Phycocyanin (PC), and Allophycocyanin (APC) from the PC-rich and PE-rich *Synechococcus* cultures. These estimations were based on established linear correlations between pigment content, determined through extraction methods (Strickland and Parsons 1972; Bennett and Bogorad 1973), and absorbance values of individual pigment peaks (Car; 480 nm, PE; 565 nm, PC; 620 nm, APC; 650 nm, and Chl *a*; 665 nm) obtained from whole-cell absorbance spectra (Table S2). Additionally, we summed PE, PC, and APC protein to total Phycobiliproteins content.

Using whole-cell absorbance spectra of *Synechococcus* cultures, we also estimated Photosynthetically Usable Radiation (PUR; µmol photons $m^{-2}s^{-1}$) according to (Morel 1978).

160

161 PSII effective absorption cross section of PSII, turnover time of PSII
162 photochemistry, and photochemical quenching

163 We harvested 4 mL of picocyanobacteria cultures repeatedly across the growth trajectories
164 for photophysiological characterizations. For the low oxygen cultures, to ensure
165 photophysiological measurements were taken at low O_2 of ~ 2.5 µM, we bubbled gently with N_2
166 from a gas cylinder during measurements. [O_2] was verified in culture samples for
167 photophysiological measurements using oxygen optodes (PyroScience, Germany) inserted (data
168 not presented).

169 We used Fast Repetition & Relaxation chlorophyll fluorescence (FRRf) (Kolber et al. 1998)
170 (Solisense, USA), with a lab built temperature control jacket (22℃), to apply a series of 100
171 excitation flashlets of 1.6 µs to drive saturation of PSII variable fluorescence, followed
172 immediately by logarithmically spaced flashlets to track relaxation of variable fluorescence.
173 Induction/relaxation trajectories were fit using the onboard Solisense LIFT software (Falkowski
174 and Kolber 1993; Kolber et al. 1998).

175 We used a double tap protocol (Xu et al. 2017), where FRRf induction/relaxation trajectories
176 were collected during a rapid actinic light curve sequence increasing in steps of 10 s at 0, 20, 40,
177 80, 160, and 320 µmol photons $m^{-2}s^{-1}$ PAR. We applied 1 s darkness between the sequential 10 s
178 steps of the light response curves, to allow re-opening of PSII immediately after application of the
179 sequential increasing light steps. Flashlets and actinic light were delivered from LED emitters
180 centred at Ex_{445nm}, preferentially exciting chlorophyll; Ex_{470nm}, preferentially exciting
181 phycourobilin (PUB); Ex_{535nm}, preferentially exciting phycoerythrin (PE); or Ex_{590nm},
182 preferentially exciting phycocyanin (PC). Excitation flashlets and actinic light wavebands were

matched for each run. These actinic and excitation wavebands in turn approximated 4 of our 7 growth light wavebands (450, 470, 530 & 620 nm), allowing us to evaluate *in situ* photosynthetic performance for those culture conditions.

Flashlet power delivered to the samples during the 1.6 µs flashlet duration was adjusted to achieve saturation of variable fluorescence; Ex_{445nm} at 60000 µmol photons $m^{-2}s^{-1}$ PAR; Ex_{470nm} at 30000 µmol photons $m^{-2}s^{-1}$ PAR; Ex_{535nm} at 25000 µmol photons $m^{-2}s^{-1}$ PAR; while for Ex_{590nm} excitation power at 14000 µmol photons $m^{-2}s^{-1}$, calibrated using a quantum sensor (LI-250, LI-COR, Inc.) in the temperature controlled cuvette.

We estimated effective absorption cross section of PSII (σ_{PSII}; nm^2 $quanta^{-1}$); turnover time of PSII photochemistry (τ_{PSII}; µs); and the photochemical quenching coefficient (q_P) using the FRRf induction curves, following (Xu et al. 2017). We fit a model with three τ_{PSII} to describe the re-opening of PSII after closure by the saturating flash train. For subsequent analyses we estimated an average of the three τ_{PSII}, weighted by their respective amplitudes, to describe the overall time to reopen PSII after closure.

PSII electron flux

We calculated (Eq. (1)) an uncalibrated fluorescence based estimator for volumetric electron transport, JV_{PSII}, (k × e^- L^{-1} s^{-1}) under Ex_{445nm}, blue; Ex_{470nm}, blue-green; Ex_{535nm}, green; or Ex_{590nm}, red-orange excitation bands (Oxborough et al. 2012; Boatman et al. 2019; Tortell and Suggett 2021).

$$JV_{PSII} = \frac{\sigma_{PSII}' \times q_P \times I \times F_O}{\sigma_{PSII}} \qquad (1)$$

where σ_{PSII}' is effective absorption cross section for PSII photochemistry under the relevant actinic PAR step (nm^2 $quanta^{-1}$); q_P is an estimate of the fraction of PSII open for photochemistry

estimated according to Oxborough and Baker (1997); I is the applied PAR (µmol photons $m^{-2}s^{-1}$); F_O is the minimum fluorescence from a given sample and excitation waveband (relative fluorescence) and σ_{PSII} is the maximum effective absorption cross section for PSII photochemistry from a given sample and excitation waveband (nm^2 $quanta^{-1}$).

We calibrated the JV_{PSII} estimator to absolute rates of electron transport (Eq. (2)) using parallel measures of oxygen evolution (µmol O_2 L^{-1} s^{-1}), captured simultaneously with the FRRf measures, taken below light saturation of electron transport to limit distortion from electron fluxes back to oxygen under super-saturating light (Hughes et al. 2018), using a FireSting robust oxygen probe (PyroScience, Germany) inserted in the cuvette for select Rapid Light Curve (RLC) runs (Table S3).

$$JV_{PSII}(e^- L^{-1} s^{-1}) = \frac{Uncalibrated\ JV_{PSII}(e^- L^{-1} s^{-1})}{Calibration\ slope} \qquad (2)$$

We converted JV_{PSII} (µmol e^- L^{-1} s^{-1}) to JV_{PSII} (µmol e^- µmol Chl a^{-1} d^{-1}) by performing Chl *a* (µg L^{-1}) measurements using Trilogy Laboratory Fluorometer (Turner Designs, Inc., CA, USA) equipped with Chlorophyll In-Vivo Module, on the samples taken for the FRRf measurements.

To generate an index of the ratio of Chl *a* : PSII we divided PSII electron transport (e- $PSII^{-1}$ s^{-1}) by JV_{PSII} (e- Chl^{-1} s^{-1}), both estimated under Ex_{445nm}, with units cancelling to Chl *a* : PSII. Since the number of Chl *a* directly associated with the core of PSII is fixed, variations in Chl *a* to PSII reflect changes in the PSI:PSII ratio, and possibly the presence of other chl-containing complexes.

Statistical analysis

We used R version 4.3.0 (R Core Team 2023) running under RStudio (Posit team 2022). We performed three-way factorial ANOVA (*aov()* function; R Base package) to determine whether strain, growth waveband, and $[O_2]$ significantly influence the chlorophyll-specific growth rate (μ; d^{-1}; Table S4) or pigment content (Table S5). We also performed three-way factorial ANOVA (*aov()* function) to determine whether strain, Actinic PAR, and $[O_2]$ significantly influence the responses of σ_{PSII} (Table S6); τ_{PSII} (Table S7); q_P (Table S8); or JV_{PSII} (Table S9) to increasing light. We fit the light response curves of JV_{PSII} with a three parameter model (Harrison and Platt 1986) using (Elzhov et al. 2023) for *nlsLM()* function. Three-way factorial ANOVA (*aov()* function; R Base package) was performed to determine whether strain, growth waveband, and $[O_2]$ significantly influence Chl *a* to PSII (Table S10).

We used *t*-tests of linear regressions to compare data across different strains and $[O_2]$ for a given growth waveband, for chlorophyll-specific growth rate vs. Phycobiliproteins to Chl *a* ratio (Table S11). We also performed *t*-tests of linear fits to compare data across different strains and $[O_2]$ in situations in which cultures were excited by, and growing in, corresponding growth wavebands of 450, 470, 530, or 620 nm, for chlorophyll-specific growth rate vs. JV_{PSII} (Table S12). Statistical differences for all analyses were determined at significance level $\alpha = 0.05$.

The manuscript was prepared as a Rmarkdown document (Handel 2020) with figures plotted using ggplot2 (Wickham 2016) and patchwork (Pedersen 2024) packages. All metadata, data, and code is available on GitHub (https://github.com/FundyPhytoPhys/BalticO2).

Results

Chlorophyll-specific growth rates across [O_2], spectral wavebands, and strains

We used logistic curve fits (Fig. S1) to determine chlorophyll-specific growth rates (μ; d^{-1}) for PC-rich and PE-rich cultures of *Synechococcus* grown under spectral wavebands centred at 405, 450, 470, 530, 620, 660, or 730 nm, and [O_2] of 250 μM or 2.5 μM (Fig. 1). Growth curves, tracked as OD_{680}, OD_{720}, ΔOD and logistic fits of ΔOD vs. elapsed time are shown in Fig. S1 in Supplementary materials. Cell-specific growth rates (μ) were also determined using OD_{720} (Fig. S2). Strain, growth waveband, [O_2], and their interactions, significantly affected μ (Table S4).

PC-rich and PE-rich *Synechococcus* grow under 2.5 μM [O_2], across the range of tested spectral wavebands from 405 – 730 nm. In contrast, under 250 μM [O_2], the PC-rich strain failed to grow under 405 nm, while the PE-rich strain failed to grow under 405, 450, and 730 nm. The PC-rich strain showed generally similar growth rates under 2.5 and 250 μM [O_2], across tested spectral wavebands (nm). In contrast the PE-rich strain achieved faster growth rates under 2.5 μM [O_2] than under 250 μM [O_2].

PC-rich *Synechococcus* showed a peak in growth rate under both [O_2] and red light of 620 or 660 nm, absorbed by phycocyanin and chlorophyll. Under 2.5 μM [O_2] the PE-rich strain showed high growth rates under 530 nm – 660 nm absorbed by phycoerythin, phycocyanin, and chlorophyll; while under 250 μM [O_2], the PE-rich strain showed the highest growth rate under green light of 530 nm absorbed by phycoerythrin.

Fig. 1. Chlorophyll-specific growth rates (μ; d^{-1}) vs. growth waveband (nm, shaded regions). Growth rates (± SE) were estimated from logistic fits of chlorophyll proxy $OD_{680} - OD_{720}$ (ΔOD) vs. elapsed time (Fig. S1), for PC-rich (green circle) and PE-rich (red circle) cultures of

272 *Synechococcus* grown at spectral wavebands of 405, 450, 470, 530, 620, 660, or 730 nm, and [O_2]
273 of 250 µM (open symbols and dashed line) or 2.5 µM (closed symbols and solid line).
274

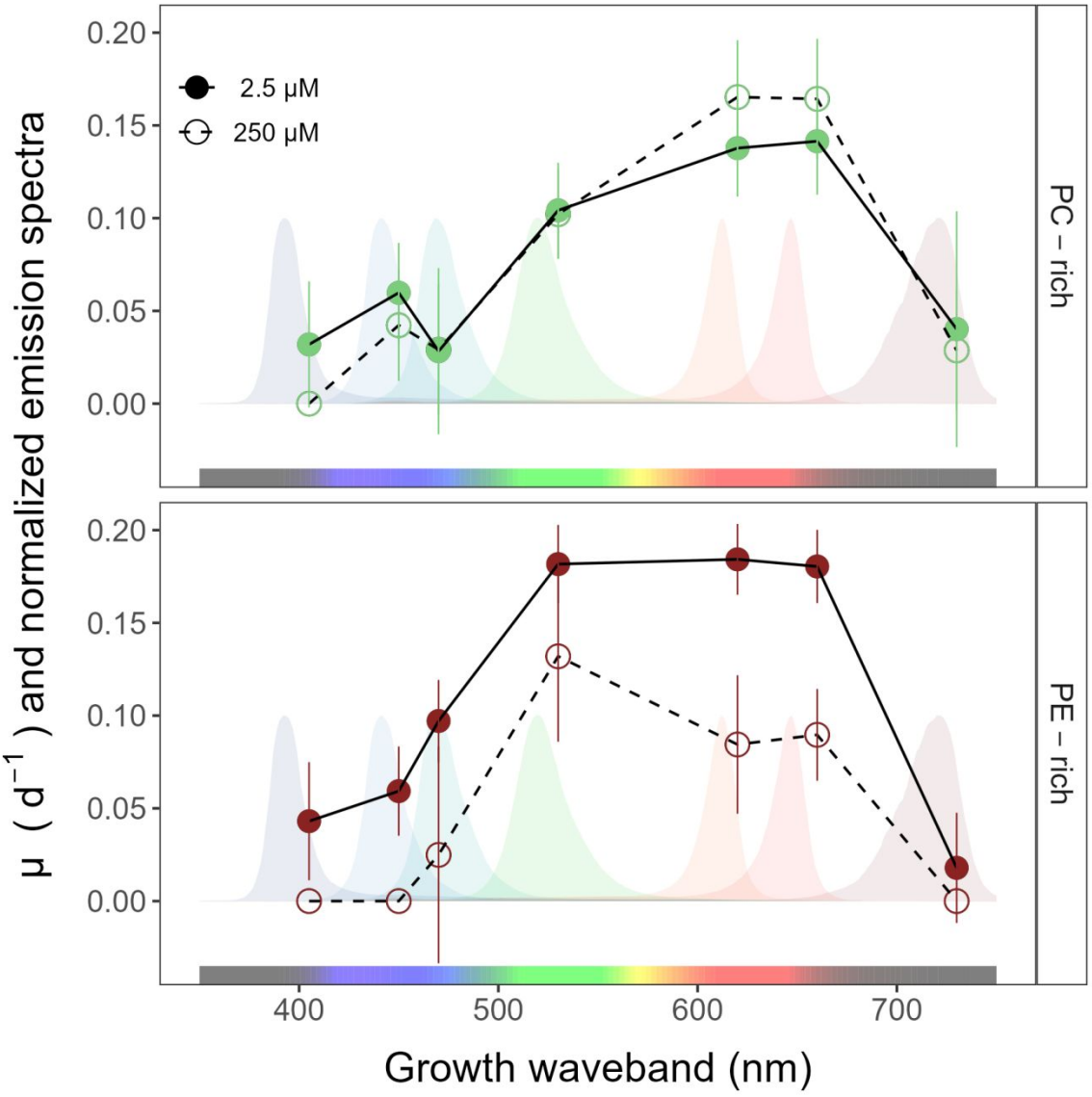

275
276

277 Pigment content and pigment ratio across [O_2], spectral wavebands, and strains

278 Fig. 2*a* presents Chlorophyll *a* (Chl *a*), Phycobiliproteins (Phyco), or Carotenoids (Car)
279 content (pg cell $^{-1}$) vs. growth waveband (nm) for PC-rich and PE-rich cultures of *Synechococcus*

grown at spectral wavebands centred at 405, 450, 470, 530, 620, 660, or 730 nm and 250 or 2.5 μM [O_2]. We also calculated the Car to Chl *a* ratio, and the ratio of the sum of Phycobiliproteins to Chl *a* (μg:μg) for each strain (Fig. S3). Moreover, phycobiliproteins:Chlorophyll *a* ratio (μg:μg) and chlorophyll-specific growth rates (μ; d^{-1}) vs. Photosynthetically Usable Radiation (PUR, μmol photons $m^{-2}s^{-1}$) for PC-rich and PE-rich cultures of *Synechococcus* grown at spectral wavebands of 405, 450, 470, 530, 620, 660, or 730 nm and 250 μM [O_2] or 2.5 μM [O_2] are presented in Fig. S4.

To focus on the responses of growing cells, we omit pigmentation data from those PE-rich cultures which showed negligible growth under 405, 450, 730 nm and 250 μM [O_2]; and from those PC-rich cultures which showed negligible growth under 405 nm and 250 μM [O_2].

Strain, growth waveband, [O_2], and their interactions, significantly affected cell-specific Chl *a*, Phycobiliproteins, and Car content (Table S5). For the PC-rich strain, the highest Chl *a*, Phycobiliproteins, and Car contents were recorded after growth under 730 nm. The phycobiliproteins content was higher under 250 μM [O_2] than under 2.5 μM [O_2] for the PC-rich strain. In contrast, for PE-rich *Synechococcus*, phycobiliproteins content was significantly lower under 250 μM [O_2] than under 2.5 μM [O_2], with the highest phycobiliproteins content under 620 nm and 2.5 μM [O_2].

Chlorophyll-specific growth rates (μ; d^{-1}) show positive linear responses to the Phycobiliproteins:Chlorophyll *a* ratio (μg:μg), for both PC-rich and PE-rich *Synechococcus* (Fig. 2*b*), although the relations vary across strain and [O_2] (Table S11).

Fig. 2. Pigment content (pg cell $^{-1}$) vs. growth waveband (nm) (*a*) and Chlorophyll-specific growth rates (μ; d^{-1}) vs. Phycobiliproteins:Chlorophyll *a* ratio (μg:μg) (*b*) for PC-rich (green circle) and

PE-rich (red circle) cultures of *Synechococcus* grown at spectral wavebands of 405, 450, 470, 530, 620, 660, or 730 nm and 250 μM [O_2] (open symbols and dashed line) or 2.5 μM [O_2] (closed symbols and solid line). Data not presented for those PE-rich cultures which showed negligible growth under 405, 450, 730 nm and 250 μM [O_2]; nor for those PC-rich cultures which showed negligible growth under 405 nm and 250 μM [O_2]. Blue lines shows linear model fit for data from each strain and [O_2] (solid for 2.5 μM [O_2] or dashed for 250 μM [O_2]) across spectral wavebands. Different blue lowercase letters indicate statistically significant differences between the fit models for different [O_2] within a given strain. Different blue uppercase letters indicate statistically significant differences between the fit models for different strains within a given [O_2] (*t*-test; $p < 0.05$).

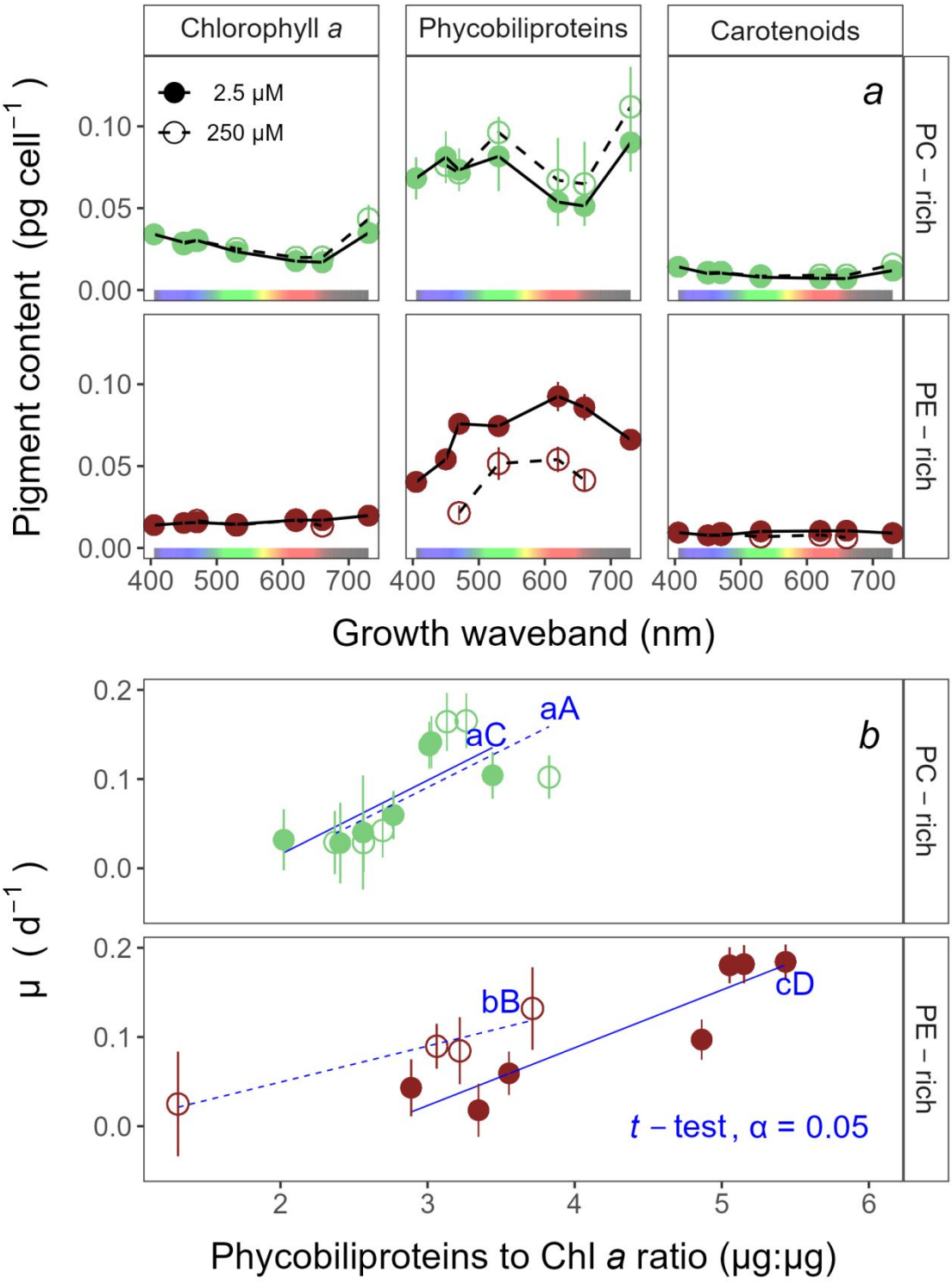

314

315

Effective absorption cross sections, turnover times, and photochemical quenching of PSII across [O_2], spectral wavebands, and strains

Light response curves of effective absorption cross section of PSII (σ_{PSII}; nm^2 $quanta^{-1}$); turnover time of PSII photochemistry (τ_{PSII}; µs); and the photochemical quenching coefficient (q_P) vs. Actinic PAR (µmol photons $m^{-2}s^{-1}$) (Fig. 3*a-c*) are shown for PC-rich and PE-rich cultures grown in, and excited by, corresponding wavebands of 450, 470, 530, or 620 nm, at 250 µM or 2.5 µM [O_2]. We omit functional data determined for those PE-rich cultures which showed negligible growth under 405, 450, 730 nm and 250 µM O_2; and for those PC-rich cultures which showed negligible growth under 405 nm and 250 µM O_2. In the Supplementary materials (Fig S5-S7), we also show the light response curves for all available excitation (Ex_{445nm}, blue; Ex_{470nm}, blue-green; Ex_{535nm}, green; or Ex_{590nm}, orange) and growth waveband (450, 470, 530, or 620 nm) cross-combinations.

σ_{PSII} (Fig. 3*a*), a measure of excitation driving PSII photochemistry, was low and shows little change with increasing actinic light during excitation through chlorophyll at Ex_{445nm}. For the PC-rich strain, under orange excitation at Ex_{590nm}, σ_{PSII} showed an initial small increase from darkness to the growth light level, followed by a mild decrease with increasing Actinic PAR, and was higher at 250 µM [O_2] compared to 2.5 µM [O_2]. For the PE-rich strain, we again see a small increase from darkness to the growth light level, followed by a decrease in σ_{PSII} with increasing Actinic PAR. Moreover, for the PE-rich strain σ_{PSII} was higher in low [O_2] conditions than in high [O_2] conditions. Strain, Actinic PAR, and [O_2] significantly influenced σ_{PSII} under excitation at Ex_{590nm} (Table S6).

For the PC-rich strain, across the excitation wavebands tested, τ_{PSII} showed an acceleration (decrease) from darkness to growth light Actinic PAR (Fig. 3*b*), to a plateau of ~ 800 µs. PE-rich

strains, on the other hand, showed a progressive acceleration (decrease) with increasing Actinic PAR under excitation at Ex_{470nm}, Ex_{535nm}, or Ex_{590nm}, declining towards ~ 400 µs under Ex_{590nm}. Thus, the PE-rich strain showed more capacity to remove electrons from PSII. τ_{PSII}, was generally faster (smaller) for both PC-rich and PE-rich strains under 250 µM $[O_2]$. Strain, Actinic PAR, and $[O_2]$ significantly affected τ_{PSII} at Ex_{470nm}, Ex_{535nm} and Ex_{590nm} (Table S7).

q_P, a measure of the fraction of PSII available for photochemistry, showed a strong decrease with increasing Actinic PAR across the excitation wavebands tested (Fig. 3*c*). q_P generally remained higher for both PC-rich and PE-rich strains under 250 µM $[O_2]$. Strain, Actinic PAR, and $[O_2]$ significantly affected q_P at Ex_{470nm}, Ex_{535nm}, and Ex_{590nm} (Table S8).

Fig. 3. Effective absorption cross section of PSII (σ_{PSII}; nm^2 $quanta^{-1}$) (*a*); turnover time of PSII photochemistry (τ_{PSII}; µs) (*b*); or photochemical quenching coefficient (q_P) (*c*) vs. Actinic PAR (µmol photons $m^{-2}s^{-1}$). Parameters were estimated using FRRf induction curves with excitation (columns) at Ex_{445nm}, blue; Ex_{470nm}, blue-green; Ex_{535nm}, green; or Ex_{590nm}, orange; for PC-rich (green circle) or PE-rich (red circle) cultures of *Synechococcus*. Data show situations in which cultures were excited by, and growing in, corresponding growth wavebands of 450, 470, 530, or 620 nm and 250 µM $[O_2]$ (open symbols and dashed line) or 2.5 µM $[O_2]$ (closed symbols and solid line). The vertical lines show half diel peak PAR growth light of 90 µmol photons $m^{-2}s^{-1}$. Data not presented for those PE-rich cultures which showed negligible growth under 405, 450, 730 nm and 250 µM O_2; nor for those PC-rich cultures which showed negligible growth under 405 nm and 250 µM O_2.

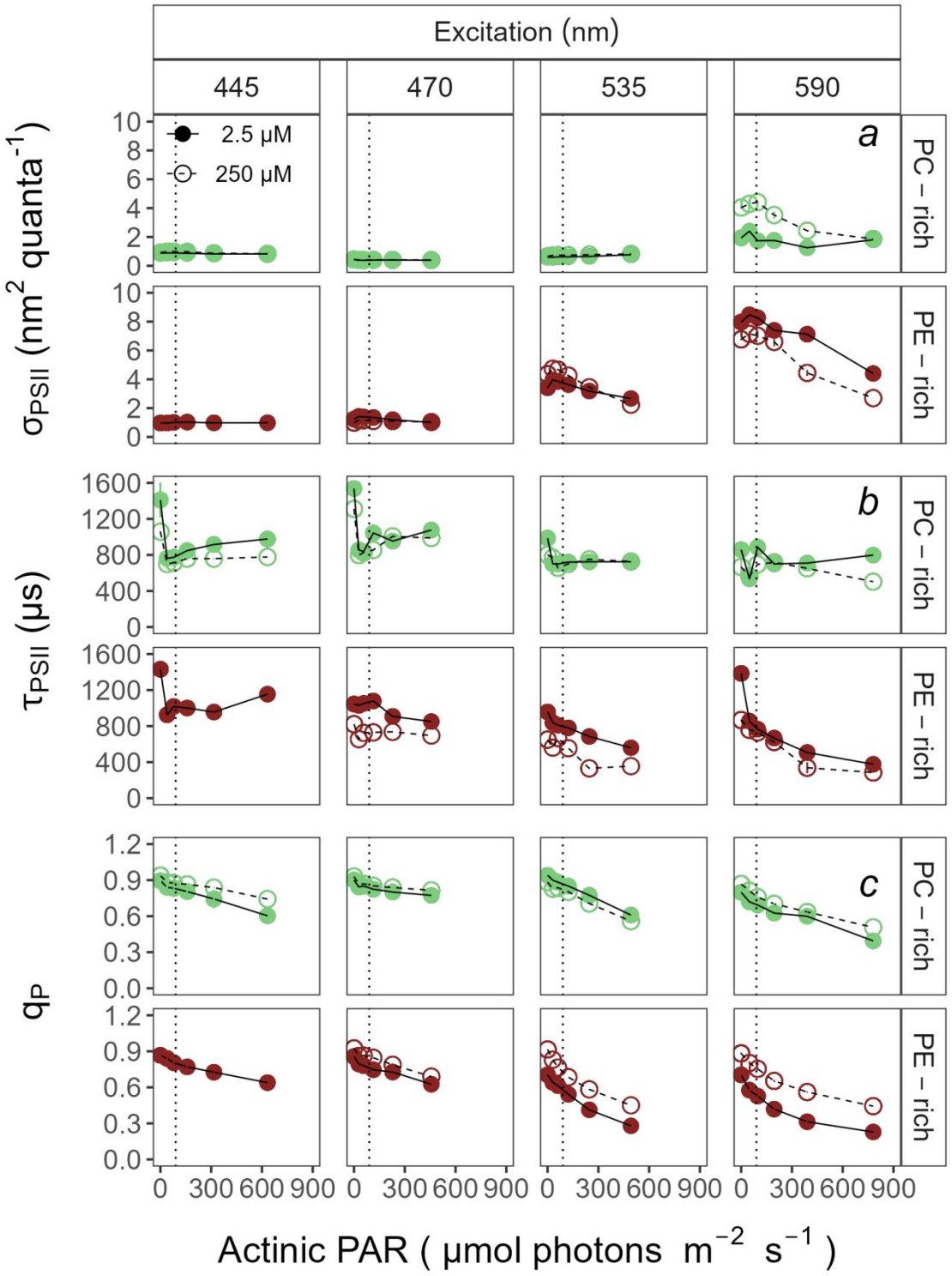

361

362

PSII electron flux across [O_2], spectral wavebands, and strains

PSII electron flux (JV_{PSII}) measures the generation of reductant available to support biosynthetic assimilation and growth. JV_{PSII} was estimated using FRRf inductions with excitation at Ex_{445nm}, Ex_{470nm}, Ex_{535nm}, or Ex_{590nm}, corresponding to growth wavebands of 450, 470, 530, or 620 nm and 250 µM or 2.5 µM [O_2]. To focus on responses of growing cells, we do not present JV_{PSII} data for those PE-rich cultures which showed negligible growth under 405, 450, 730 nm and 250 µM O_2; nor for those PC-rich cultures which showed negligible growth under 405 nm and 250 µM O_2. PSII electron flux (JV_{PSII}; µmol e^- µmol Chl a^{-1} s^{-1}) vs. Actinic PAR (µmol photons $m^{-2}s^{-1}$) estimated using FRRf induction curves with excitation at Ex_{445nm}, blue; Ex_{470nm}, blue-green; Ex_{535nm}, green; or Ex_{590nm}, orange; for PC-rich or PE-rich cultures of *Synechococcus* grown at spectral bandwidths of 450, 470, 530, or 620 nm and O_2 concentrations of 250 µM or 2.5 µM are also presented (Fig. S8).

Light response curves of PSII electron flux (JV_{PSII}; µmol e^- µmol Chl a^{-1} s^{-1}) vs. Actinic PAR (µmol photons $m^{-2}s^{-1}$) are shown in Fig. 4*a*. For the PC-rich strain, under all tested excitations (Ex_{445nm}, Ex_{470nm}, Ex_{535nm}, or Ex_{590nm}), JV_{PSII} increased with increasing Actinic PAR, and did not fully saturate across the range of tested actinic PAR. Under all excitations, except Ex_{590nm}, JV_{PSII} was higher at 2.5 µM [O_2] compared to 250 µM [O_2] for the PC-rich strain. Conversely, for the PE-rich strain, JV_{PSII} under Ex_{470nm}, Ex_{535nm}, or Ex_{590nm} was higher at 250 µM [O_2] compared to 2.5 µM [O_2]. Moreover, for the PE-rich strain, JV_{PSII} plateaued above ~90 µmol photons $m^{-2}s^{-1}$ under Ex_{535nm}, or Ex_{590nm} for both low and high [O_2]. Strain, Actinic PAR, and [O_2] significantly influence JV_{PSII} under some of the tested excitations (Table S9), but JV_{PSII} for cultures grown under, and excited through, Ex_{445nm}, absorbed by chlorophyll, shows no difference between low and high [O_2] with increasing actinic light.

Fig. 4*b* presents linear regressions between chlorophyll-specific growth rates (μ; d^{-1}) and cumulative diel PSII electron flux (JV_{PSII}; μmol e^- μmol Chl a^{-1} d^{-1}) measured under half (90 μmol photons $m^{-2}s^{-1}$) of the diel peak PAR growth light. μ (d^{-1}), as expected, was positively correlated with JV_{PSII}, with slopes significantly greater than 0. [O_2] significantly influences the linear regressions between chlorophyll-specific growth rates and PSII electron flux for both PC-rich and PE-rich strains of *Synechococcus* ($p < 0.05$, Table S12). In the PC-rich strain higher [O_2] increases the growth yield of electron transport. In contrast, the PE-rich strain, under higher [O_2], decreases the growth yield of electron transport. However, the regressions for a given [O_2] are not significantly different between the two strains ($p > 0.05$, Table S12).

Strain, actinic PAR waveband, and [O_2] significantly influence Strain, Actinic PAR, and [O_2] significantly influence our metric of Chl *a* : PSII (Fig. S9, Table S10), with Chl *a* : PSII higher under 250 than under 2.5 μM [O_2] in the PC-rich strain, and Chl *a* : PSII generally lower in the PC-rich stain compared to the PE-rich strain.

Fig. 4. PSII electron flux (JV_{PSII}; μmol e^- μmol Chl a^{-1} s^{-1}) vs. Actinic PAR (μmol photons $m^{-2}s^{-1}$) (*a*). JV_{PSII} was estimated using FRRf induction curves with excitation at Ex_{445nm}, blue; Ex_{470nm}, blue-green; Ex_{535nm}, green; or Ex_{590nm}, orange; for PC-rich (green circle) or PE-rich (red circle) cultures of *Synechococcus*. Data show situations in which cultures were excited by, and growing in, corresponding growth wavebands of 450, 470, 530, or 620 nm and 250 μM [O_2] (open symbols and dashed line) or 2.5 μM [O_2] (closed symbols and solid line). JV_{PSII} vs. Actinic PAR (μmol photons $m^{-2}s^{-1}$) was fit with a Harrison and Platt Light Response Curve model (Harrison and Platt 1986), used to estimated JV_{PSII} at 90 μmol photons $m^{-2}s^{-1}$ (vertical dotted lines). Chlorophyll-specific growth rates (μ; d^{-1}) vs. PSII electron flux (JV_{PSII}; μmol e^- μmol Chl a^{-1} d^{-1}) measured

409 under half (90 µmol photons $m^{-2}s^{-1}$) of diel peak PAR growth light (*b*). Blue lines (solid for 2.5
410 µM $[O_2]$ or dashed for 250 µM O_2) show linear model fit for data from each strain across spectral
411 wavebands. Different blue lowercase letters indicate statistically significant differences between
412 the fit models for different $[O_2]$ within a given strain. Different blue uppercase letters indicate
413 statistically significant differences between the fit models for different strains within a given $[O_2]$
414 (*t*-test; $p < 0.05$).
415

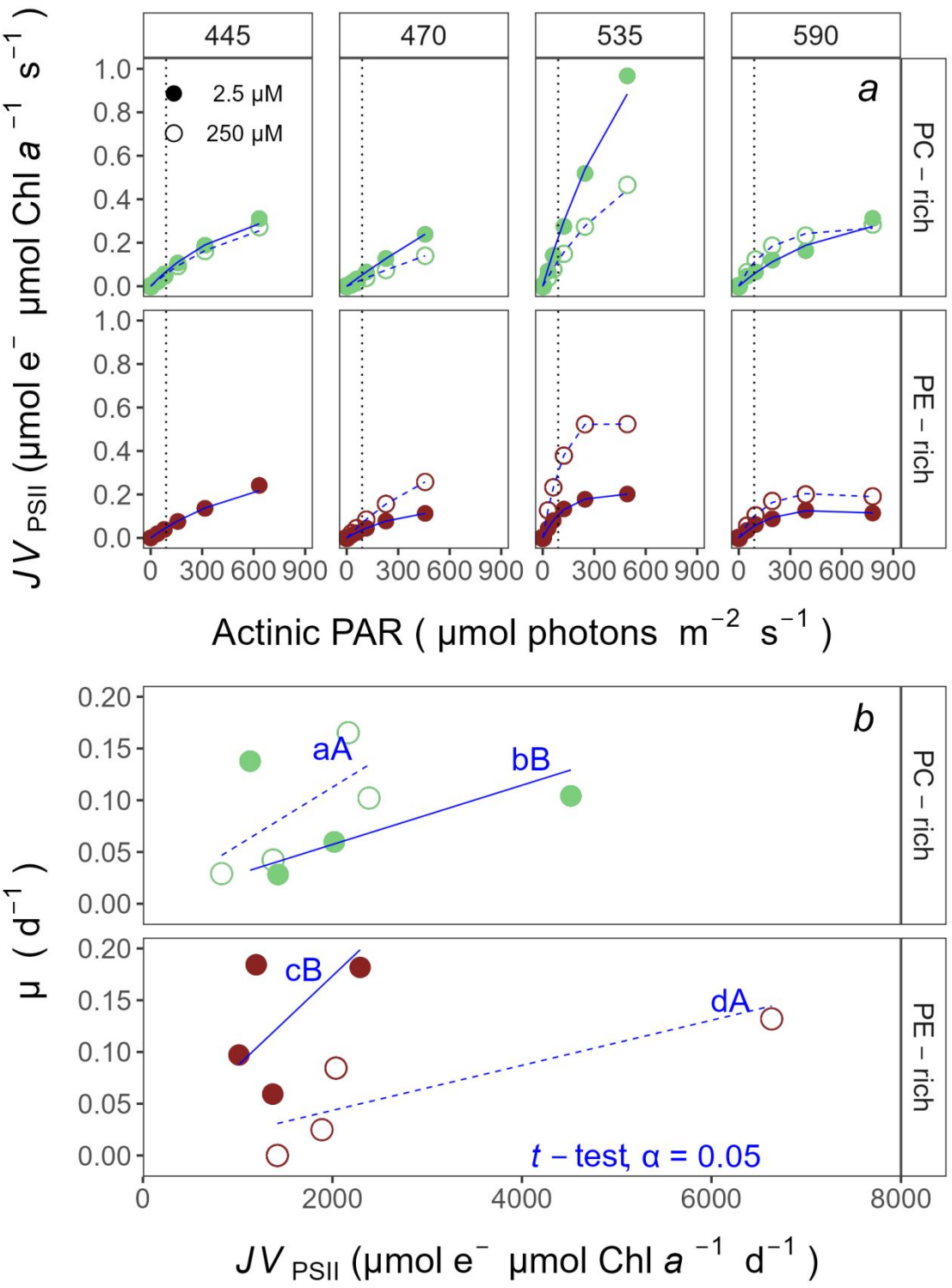

416

417

Discussion

Growth responses of PC-rich and PE-rich picocyanobacteria across [O_2] and spectral wavebands

Picocyanobacteria from the genus *Synechococcus* are major contributors to primary marine production, across a wide range of environments (Śliwińska-Wilczewska et al. 2018a; Aguilera et al. 2023) but interactive influences of [O_2] and spectral wavebands on their growth rates and ecophysiology have not yet been investigated.

PC-rich and PE-rich *Synechococcus* from coastal habitats are exposed to changes in irradiance, spectral waveband, and sometimes [O_2], by vertical movements through the mixed layer. Fluctuation in spectral wavebands changes the balance between productive photosynthesis, and photoinactivation of PSII (Six et al. 2007), increasing the cost of growth by diverting protein metabolism towards PSII repair (Murphy et al. 2017). Indeed, under 250 µM [O_2], the PC-rich strain failed to grow under 405 nm, while the PE-rich strain failed to grow under 405 and 450, consistent with accelerated photoinactivation of PSII under blue wavebands (Murphy et al. 2017). In contrast, growth persisted in both strains at 405 & 450 nm under 2.5 µM [O_2], likely because generation of toxic Reactive Oxygen Species (ROS) was suppressed, lowering the burden of photoinactivation of PSII.

µ shows positive responses to both Phycobiliproteins:Chlorophyll *a* ratio, an index of light capture capacity, and to cumulative diel PSII electron flux (JV_{PSII}) for *Synechococcus*, although the relations varied across strain and with [O_2]. In the PC-rich strain lower [O_2] lowered the yield of growth per electron flux, while in the PE-rich strain the yield of growth per electron flux increased under lower [O_2]. Note that these regressions excluded those conditions where no growth occurred. In contrast, growth showed no correlation to estimated Photosynthetically Usuable

441 Radiation (PUR) (Fig. S4), likely because of variable allocations of excitation from
442 phycobilisomes across growth conditions (Campbell 1996), not captured in the PUR metric based
443 upon light absorption.

444 Wong et al. (2023) found that vertical structures of phytoplankton communities in OMZ are
445 not sufficiently explained by top-down predation pressure nor light and/or nutrient limitation and
446 thus, some phytoplankton may have a higher than expected direct O_2 requirement, with growth
447 inhibited by low O_2 levels. However, in our work we show that low oxygen levels either do not
448 affect, or sometimes even benefit, growth of different *Synechococcus* phenotypes across spectral
449 wavebands. What is more, historical data link major extinction events to warm climates and
450 oxygen-deficient oceans, with current anthropogenic activities possibly leading to widespread
451 OMZ within a thousand years (Breitburg et al. 2018). The PC-rich *Synechococcus* strain showed
452 generally similar growth rates under high and low tested [O_2], while the PE-rich strain achieved
453 faster growth rates under low (2.5 µM) than under high (250 µM) [O_2]. PE-rich *Synechococcus*
454 are typically found at greater depths, and lower light, than are PC-rich strains (Haverkamp et al.
455 2009; Śliwińska-Wilczewska et al. 2018a) but we suggest that the PE-rich strains may actually be
456 limited to lower light niches by the interaction between light level, spectral band, and full air-
457 saturated [O_2]. In lower oxygen waters PE-rich strains will likely exploit higher light niches nearer
458 the surface.

459

460 Physiological adaptations of PC-rich and PE-rich picocyanobacteria to [O_2] and
461 spectral wavebands

462 *Synechococcus* strains vary widely in pigment composition, enabling them to exploit
463 different spectral niches (Moore et al. 1995; Six et al. 2007; Grébert et al. 2018; Efimova et al.

464 2020). With a small diameter of 0.8–2.0 µm, *Synechococcus* possess a high surface-to-volume
465 ratio (Śliwińska-Wilczewska et al. 2018b), minimizing pigment package effects (Finkel 2001), and
466 resulting in high optical absorption per pigment. This characteristic allows them to thrive under
467 low light deep in the water column (Moore et al. 1995), and to disproportionately influence sub-
468 surface light fields (Berthold and Schumann 2020). Although limited package effect increases
469 photon capture per pigment investment, it also increases *Synechococcus* susceptibility to light-
470 induced damage (Llabrés and Agustí 2006, 2010). In some *Synechococcus*, a carotenoid-protein
471 complex regulates the connectivity of the phycobilisome to the reaction center, mediating a form
472 of non-photochemical quenching of excitation (Wilson et al. 2006; Gorbunov et al. 2011;
473 Kirilovsky 2015). In our work we found no change in bulk carotenoids content (Fig. 2), nor in Car
474 to Chl *a* ratio (Fig. S3) under the different [O_2]. What is more, for the PE-rich strain, the
475 carotenoids content did not change across tested wavebands. On the other hand, for PC-rich
476 picocyanobacteria, a slight increase in carotenoids content was recorded under 405 nm, although
477 these cells were not growing and were thus under stress.

478 σ_{PSII} was low and showed little change with increasing actinic light during excitation through
479 chlorophyll at Ex_{445nm}, because in cyanobacteria the number of chlorophyll per PSII is low, and
480 nearly fixed, so the effective absorption cross section of PSII for chlorophyll is low (Xu et al.
481 2018). With excitation through the phycobilisomes at 535 and 590 nm σ_{PSII} rose to a peak near the
482 acclimated light level of ~ 90 µmol photons $m^{-2}s^{-1}$ (Campbell and Oquist 1996), reflecting the
483 state transition mechanism.

484 τ_{PSII} was generally faster for both PC-rich and PE-rich strains under 250 µM [O_2], consistent
485 with the cyanobacterial capacity for pseudo-cyclic electron flows away from PSII to [O_2]
486 (Campbell et al. 1999; Grossman et al. 2010; Allahverdiyeva et al. 2015; Hughes et al. 2018),

thereby controlling feedback inhibition of electron transport, and decreasing the risks of ROS production. In parallel,q_P was generally higher for PC-rich, and particularly for PE-rich strains, under 250 µM [O_2], since cyanobacteria show strong capacity for electron flow away from PSII to O_2 (Campbell et al. 1999; Hughes et al. 2018), particularly under excess excitation above the acclimated PAR of ~ 90 µmol photons $m^{-2}s^{-1}$. In spite of this superior electron transport performance under 250 µM [O_2] the PE-rich strain grew faster under 2.5 µM [O_2], showing an increase in the growth return upon electron transport.

Picocyanobacteria numerically dominate vast tracts of the oceans, contributing significant primary production, particularly in oligotrophic regions, but also some coastal habitats (Haverkamp 2008; Larsson et al. 2014; Doré et al. 2022; Aguilera et al. 2023). The ecological success of picoplanktonic *Synechococcus* reflects specific lineages occupying different niches to populate the world's oceans (Scanlan 2012). Picocyanobacteria species can share the light spectrum by specializing in different wavelengths (Stomp et al. 2004, 2007; Haverkamp et al. 2009). Competition models and laboratory experiments show that PE-rich picocyanobacteria outperform competitors in green light while PC-rich picocyanobacteria dominate in red light, while both species can coexist across the full spectrum (Stomp et al. 2004, 2007). We now find that spectral wavebands interact with [O_2] as determinants of growth rates across different *Synechococcus* strains, and that changing ocean [O_2] may drive different pigmentation phenotypes into changing ecological niches.

Acknowledgements

We thank Naaman M. Omar for assistance with coding, data analyses and culture maintenance; Miranda Corkum who maintained cultures and trained personnel in culture handling; Laurel Genge, and Carlie Barnhill (Mount Allison students) who assisted with R code.

Article information

Data availability statement

Data supporting this study is available on: https://github.com/FundyPhytoPhys/BalticO2 (public GitHub Repository) and https://docs.google.com/spreadsheets/d/1ZXpwR7Gfto-uRzVdXzMpQF4frbrvMLH_IyLqonFZRSw/edit#gid=0 (URL for MetaDataCatalog).

Code to perform data processing and analyses is available at https://github.com/FundyPhytoPhys/BalticO2.

Author information

Author ORCIDs

Sylwia Śliwińska-Wilczewska https://orcid.org/0000-0002-3147-6605

Mireille Savoie https://orcid.org/0009-0009-9499-6657

Douglas A. Campbell https://orcid.org/0000-0001-8996-5463

Author contributions

Conceptualization: SSW, DAC

Data curation: SSW

Formal analysis: SSW, MS, DAC

Funding acquisition: DAC

Investigation: SSW

Methodology: SSW, MS, DAC

Project administration: DAC

Resources: DAC

Supervision: DAC

Validation: SSW, MS, DAC

Visualization: SSW

Writing – original draft: SSW, MS, DAC

Competing interests

The authors declare there are no competing interests.

Funding information

This work was supported by Canada Research Chair in Phytoplankton Ecophysiology (DAC) and Latitude & Light; NSERC of Canada Discovery Grant (DAC).

Supplementary material

Supplementary data are available with the article at https://github.com/FundyPhytoPhys/BalticO2.

References

Aguilera, A., Alegria Zufia, J., Bas Conn, L., Gurlit, L., Śliwińska-Wilczewska, S., Budzałek, G., Lundin, D., Pinhassi, J., Legrand, C., and Farnelid, H. 2023. Ecophysiological analysis reveals distinct environmental preferences in closely related Baltic Sea picocyanobacteria. Environmental Microbiology **25**(9): 1674–1695. doi:10.1111/1462-2920.16384.

Allahverdiyeva, Y., Isojärvi, J., Zhang, P., and Aro, E.-M. 2015. Cyanobacterial Oxygenic Photosynthesis is Protected by Flavodiiron Proteins. Life **5**(1): 716–743. Multidisciplinary Digital Publishing Institute. doi:10.3390/life5010716.

Andersson, B., Salter, A.H., Virgin, I., Vass, I., and Styring, S. 1992. Photodamage to photosystem II - primary and secondary events. Journal of Photochemistry and Photobiology B: Biology **15**(1): 15–31. doi:10.1016/1011-1344(92)87003-R.

Bagby, S.C., and Chisholm, S.W. 2015. Response of Prochlorococcus to varying CO2:O2 ratios. The ISME Journal **9**(10): 2232–2245. doi:10.1038/ismej.2015.36.

Bennett, A., and Bogorad, L. 1973. Complementary Chromatic Adaptation in a filamentous blue-green alga. Journal of Cell Biology **58**(2): 419–435. doi:10.1083/jcb.58.2.419.

Berthold, M., and Schumann, R. 2020. Phosphorus Dynamics in a Eutrophic Lagoon: Uptake and Utilization of Nutrient Pulses by Phytoplankton. Frontiers in Marine Science **7**. Frontiers. doi:10.3389/fmars.2020.00281.

Blake, R., and Griff, M. 2012. In situ spectroscopy on intact *Leptospirillum Ferrooxidans* reveals that reduced cytochrome 579 is an obligatory intermediate in the aerobic iron respiratory chain. Frontiers in Microbiology **3**. [accessed 13 June 2023].

572 Boatman, T.G., Geider, R.J., and Oxborough, K. 2019. Improving the accuracy of Single Turnover
573 Active Fluorometry (STAF) for the estimation of Phytoplankton Primary Productivity (PhytoPP).
574 Frontiers in Marine Science **6**. Frontiers. doi:10.3389/fmars.2019.00319.

575 Breitburg, D., Levin, L.A., Oschlies, A., Grégoire, M., Chavez, F.P., Conley, D.J., Garçon, V.,
576 Gilbert, D., Gutiérrez, D., Isensee, K., Jacinto, G.S., Limburg, K.E., Montes, I., Naqvi, S.W.A.,
577 Pitcher, G.C., Rabalais, N.N., Roman, M.R., Rose, K.A., Seibel, B.A., Telszewski, M., Yasuhara,
578 M., and Zhang, J. 2018. Declining oxygen in the global ocean and coastal waters. Science
579 **359**(6371): eaam7240. American Association for the Advancement of Science.
580 doi:10.1126/science.aam7240.

581 Callieri, C., Cabello-Yeves, P.J., and Bertoni, F. 2022. The "Dark Side" of Picocyanobacteria: Life
582 as We Do Not Know It (Yet). Microorganisms **10**(3): 546. Multidisciplinary Digital Publishing
583 Institute. doi:10.3390/microorganisms10030546.

584 Campbell, D. 1996. Complementary chromatic adaptation alters photosynthetic strategies in the
585 cyanobacterium Calothrix. Microbiology **142**(5): 1255–1263. Microbiology Society,.
586 doi:10.1099/13500872-142-5-1255.

587 Campbell, D., Clarke, A.K., Gustafsson, P., and Öquist, G. 1999. Oxygen-dependent electron flow
588 influences photosystem II function and psbA gene expression in the cyanobacterium
589 Synechococcus sp. PCC 7942. Physiologia Plantarum **105**(4): 746–755. doi:10.1034/j.1399-
590 3054.1999.105420.x.

591 Campbell, D., and Oquist, G. 1996. Predicting Light Acclimation in Cyanobacteria from
592 Nonphotochemical Quenching of Photosystem II Fluorescence, Which Reflects State Transitions
593 in These Organisms. Plant Physiology **111**(4): 1293–1298. doi:10.1104/pp.111.4.1293.

Doré, H., Leconte, J., Guyet, U., Breton, S., Farrant, G.K., Demory, D., Ratin, M., Hoebeke, M., Corre, E., Pitt, F.D., Ostrowski, M., Scanlan, D.J., Partensky, F., Six, C., and Garczarek, L. 2022. Global Phylogeography of Marine Synechococcus in Coastal Areas Reveals Strong Community Shifts. mSystems **7**(6): e00656–22. American Society for Microbiology. doi:10.1128/msystems.00656-22.

Efimova, T.V., Churilova, T.Ya., and Mukhanov, V.S. 2020. The Influence of Light of Different Spectral Qualities on the Photosynthetic Characteristics of C-Phycocyanine-Containing Cyanobacteria Synechococcus sp. WH5701. Russian Journal of Marine Biology **46**(2): 105–112. doi:10.1134/S1063074020020042.

Elzhov, T.V., Mullen, K.M., Spiess, A.-N., and Bolker, B. 2023, September. Minpack.lm: R Interface to the Levenberg-Marquardt Nonlinear Least-Squares Algorithm Found in MINPACK, Plus Support for Bounds. [accessed 15 March 2024].

Falkowski, P.G., Katz, M.E., Knoll, A.H., Quigg, A., Raven, J.A., Schofield, O., and Taylor, F.J.R. 2004. The Evolution of Modern Eukaryotic Phytoplankton. Science **305**(5682): 354–360. American Association for the Advancement of Science. doi:10.1126/science.1095964.

Falkowski, P., and Kolber, Z. 1993. Estimation of phytoplankton photosynthesis by active fluorescence. ICES Marine Science Symposium **197**: 92–103.

Finkel, Z.V. 2001. Light absorption and size scaling of light-limited metabolism in marine diatoms. Limnology and Oceanography **46**(1): 86–94. doi:10.4319/lo.2001.46.1.0086.

Flombaum, P., Gallegos, J.L., Gordillo, R.A., Rincón, J., Zabala, L.L., Jiao, N., Karl, D.M., Li, W.K.W., Lomas, M.W., Veneziano, D., Vera, C.S., Vrugt, J.A., and Martiny, A.C. 2013. Present

and future global distributions of the marine Cyanobacteria *Prochlorococcus* and *Synechococcus*. Proceedings of the National Academy of Sciences **110**(24): 9824–9829. Proceedings of the National Academy of Sciences. doi:10.1073/pnas.1307701110.

Gorbunov, M.Y., Kuzminov, F.I., Fadeev, V.V., Kim, J.D., and Falkowski, P.G. 2011. A kinetic model of non-photochemical quenching in cyanobacteria. Biochimica et Biophysica Acta (BBA) - Bioenergetics **1807**(12): 1591–1599. doi:10.1016/j.bbabio.2011.08.009.

Grébert, T., Doré, H., Partensky, F., Farrant, G.K., Boss, E.S., Picheral, M., Guidi, L., Pesant, S., Scanlan, D.J., Wincker, P., Acinas, S.G., Kehoe, D.M., and Garczarek, L. 2018. Light color acclimation is a key process in the global ocean distribution of Synechococcus cyanobacteria. Proceedings of the National Academy of Sciences **115**(9): E2010–E2019. Proceedings of the National Academy of Sciences. doi:10.1073/pnas.1717069115.

Grossman, A.R., Mackey, K.R.M., and Bailey, S. 2010. A Perspective on Photosynthesis in the Oligotrophic Oceans: Hypotheses Concerning Alternate Routes of Electron Flow1. Journal of Phycology **46**(4): 629–634. doi:10.1111/j.1529-8817.2010.00852.x.

Guillard, R.R.L. 1975. Culture of phytoplankton for feeding marine invertebrates. *In* Culture of Marine Invertebrate Animals: Proceedings — 1st Conference on Culture of Marine Invertebrate Animals Greenport. *Edited by* W.L. Smith and M.H. Chanley. Springer US, Boston, MA. pp. 29–60. doi:10.1007/978-1-4615-8714-9_3.

Hakala, M., Tuominen, I., Keränen, M., Tyystjärvi, T., and Tyystjärvi, E. 2005. Evidence for the role of the oxygen-evolving manganese complex in photoinhibition of Photosystem II. Biochimica et Biophysica Acta (BBA) - Bioenergetics **1706**(1): 68–80. doi:10.1016/j.bbabio.2004.09.001.

636 Handel, A. 2020, October. Andreas Handel - Custom Word formatting using R Markdown.
637 https://www.andreashandel.com/posts/2020-10-07-custom-word-format/. [accessed 13 June
638 2023].

639 Harrison, W.G., and Platt, T. 1986. Photosynthesis-irradiance relationships in polar and temperate
640 phytoplankton populations. Polar biology **5**: 153–164. Springer. [accessed 15 March 2024].

641 Haverkamp, T.H.A. 2008. Shades of red and green : The colorful diversity and ecology of
642 picocyanobacteria in the Baltic Sea. YersekeNetherlands Institute of Ecology (NIOO) - Royal
643 Netherlands Academy of Arts and Sciences. [accessed 3 July 2024].

644 Haverkamp, T.H.A., Schouten, D., Doeleman, M., Wollenzien, U., Huisman, J., and Stal, L.J.
645 2009. Colorful microdiversity of Synechococcus strains (picocyanobacteria) isolated from the
646 Baltic Sea. The ISME Journal **3**(4): 397–408. doi:10.1038/ismej.2008.118.

647 Hughes, D.J., Campbell, D.A., Doblin, M.A., Kromkamp, J.C., Lawrenz, E., Moore, C.M.,
648 Oxborough, K., Prášil, O., Ralph, P.J., Alvarez, M.F., and Suggett, D.J. 2018. Roadmaps and
649 Detours: Active Chlorophyll-a Assessments of Primary Productivity Across Marine and
650 Freshwater Systems. Environmental Science & Technology **52**(21): 12039–12054. American
651 Chemical Society. doi:10.1021/acs.est.8b03488.

652 Jávorfi, T., Erostyák, J., Gál, J., Buzády, A., Menczel, L., Garab, G., and Razi Naqvi, K. 2006.
653 Quantitative spectrophotometry using integrating cavities. Journal of Photochemistry and
654 Photobiology B: Biology **82**(2): 127–131. doi:10.1016/j.jphotobiol.2005.10.002.

Keeling, R.F., Körtzinger, A., and Gruber, N. 2010. Ocean Deoxygenation in a Warming World. Annual Review of Marine Science **2**(Volume 2, 2010): 199–229. Annual Reviews. doi:10.1146/annurev.marine.010908.163855.

Kirilovsky, D. 2015. Modulating energy arriving at photochemical reaction centers: Orange carotenoid protein-related photoprotection and state transitions. Photosynthesis Research **126**(1): 3–17. doi:10.1007/s11120-014-0031-7.

Kolber, Z.S., Prášil, O., and Falkowski, P.G. 1998. Measurements of variable chlorophyll fluorescence using fast repetition rate techniques: Defining methodology and experimental protocols. Biochimica et Biophysica Acta (BBA) - Bioenergetics **1367**(1): 88–106. doi:10.1016/S0005-2728(98)00135-2.

Larsson, J., Celepli, N., Ininbergs, K., Dupont, C.L., Yooseph, S., Bergman, B., and Ekman, M. 2014. Picocyanobacteria containing a novel pigment gene cluster dominate the brackish water Baltic Sea. The ISME Journal **8**(9): 1892–1903. doi:10.1038/ismej.2014.35.

Latala, A., Jodlowska, S., and Pniewski, F. 2006. Culture Collection of Baltic Algae (CCBA) and characteristic of some strains by factorial experiment approach. Archiv fur Hydrobiologie **122**: 137–154. [accessed 19 June 2024].

Llabrés, M., and Agustí, S. 2006. Picophytoplankton cell death induced by UV radiation: Evidence for oceanic Atlantic communities. Limnology and Oceanography **51**(1): 21–29. doi:10.4319/lo.2006.51.1.0021.

674 Llabrés, M., and Agustí, S. 2010. Effects of ultraviolet radiation on growth, cell death and the
675 standing stock of Antarctic phytoplankton. Aquatic Microbial Ecology **59**(2): 151–160.
676 doi:10.3354/ame01392.

677 Luimstra, V.M., Schuurmans, J.M., Verschoor, A.M., Hellingwerf, K.J., Huisman, J., and
678 Matthijs, H.C.P. 2018. Blue light reduces photosynthetic efficiency of cyanobacteria through an
679 imbalance between photosystems I and II. Photosynthesis Research **138**(2): 177–189.
680 doi:10.1007/s11120-018-0561-5.

681 Moore, L.R., Goericke, R., and Chisholm, S.W. 1995. Comparative physiology of Synechococcus
682 and Prochlorococcus: Influence of light and temperature on growth, pigments, fluorescence and
683 absorptive properties. Marine Ecology Progress Series **116**(1/3): 259–275. Inter-Research Science
684 Center. Available from https://www.jstor.org/stable/44635011 [accessed 1 July 2024].

685 Morel, A. 1978. Available, usable, and stored radiant energy in relation to marine photosynthesis.
686 Deep Sea Research **25**(8): 673–688. doi:10.1016/0146-6291(78)90623-9.

687 Murphy, C.D., Roodvoets, M.S., Austen, E.J., Dolan, A., Barnett, A., and Campbell, D.A. 2017.
688 Photoinactivation of Photosystem II in Prochlorococcus and Synechococcus. PLOS ONE **12**(1):
689 e0168991. Public Library of Science. doi:10.1371/journal.pone.0168991.

690 Oxborough, K., and Baker, N.R. 1997. Resolving chlorophyll *a* fluorescence images of
691 photosynthetic efficiency into photochemical and non-photochemical components – calculation of
692 qP and Fv-/Fm-; without measuring Fo-; Photosynthesis Research **54**(2): 135–142.
693 doi:10.1023/A:1005936823310.

694 Oxborough, K., Moore, C.M., Suggett, D.J., Lawson, T., Chan, H.G., and Geider, R.J. 2012. Direct
695 estimation of functional PSII reaction center concentration and PSII electron flux on a volume
696 basis: A new approach to the analysis of Fast Repetition Rate fluorometry (FRRf) data. Limnology
697 and Oceanography: Methods **10**(3): 142–154. doi:10.4319/lom.2012.10.142.

698 Partensky, F., Mella-Flores, D., Six, C., Garczarek, L., Czjzek, M., Marie, D., Kotabová, E.,
699 Felcmanová, K., and Prášil, O. 2018. Comparison of photosynthetic performances of marine
700 picocyanobacteria with different configurations of the oxygen-evolving complex. Photosynthesis
701 Research **138**(1): 57–71. doi:10.1007/s11120-018-0539-3.

702 Pedersen, T.L. 2024, January. Patchwork: The Composer of Plots. [accessed 20 April 2024].

703 Posit team. 2022. RStudio: Integrated development environment for r. Posit Software, PBC,
704 Boston, MA. Available from http://www.posit.co/.

705 R Core Team. 2023. R: A language and environment for statistical computing. R Foundation for
706 Statistical Computing, Vienna, Austria. Available from https://www.R-project.org/.

707 Scanlan, D.J. 2012. Marine Picocyanobacteria. *In* Ecology of Cyanobacteria II: Their Diversity in
708 Space and Time. *Edited by* B.A. Whitton. Springer Netherlands, Dordrecht. pp. 503–533.
709 doi:10.1007/978-94-007-3855-3_20.

710 Six, C., Finkel, Z.V., Irwin, A.J., and Campbell, D.A. 2007. Light variability illuminates niche-
711 partitioning among marine picocyanobacteria. PLOS ONE **2**(12): e1341. Public Library of
712 Science. doi:10.1371/journal.pone.0001341.

713 Śliwińska-Wilczewska, S., Cieszyńska, A., Maculewicz, J., and Latała, A. 2018a.
714 Ecophysiological characteristics of red, green, and brown strains of the Baltic picocyanobacterium

Synechococcus sp. – a laboratory study. Biogeosciences **15**(20): 6257–6276. Copernicus GmbH. doi:10.5194/bg-15-6257-2018.

Śliwińska-Wilczewska, S., Maculewicz, J., Barreiro Felpeto, A., and Latała, A. 2018b. Allelopathic and bloom-forming picocyanobacteria in a changing world. Toxins **10**(1): 48. Multidisciplinary Digital Publishing Institute. doi:10.3390/toxins10010048.

Stomp, M., Huisman, J., de Jongh, F., Veraart, A.J., Gerla, D., Rijkeboer, M., Ibelings, B.W., Wollenzien, U.I.A., and Stal, L.J. 2004. Adaptive divergence in pigment composition promotes phytoplankton biodiversity. Nature **432**(7013): 104–107. Nature Publishing Group. doi:10.1038/nature03044.

Stomp, M., Huisman, J., Vörös, L., Pick, F.R., Laamanen, M., Haverkamp, T., and Stal, L.J. 2007. Colourful coexistence of red and green picocyanobacteria in lakes and seas. Ecology Letters **10**(4): 290–298. doi:10.1111/j.1461-0248.2007.01026.x.

Strickland, J.D., and Parsons, T.R. 1972. Practical Hand Book of Seawater Analysis. Fisheries Research Board of Canada **167 (2nd edition)**: 1–311. doi:DOI: http://dx.doi.org/10.25607/OBP-1791.

Tortell, P., and Suggett, D.J. 2021. A user guide for the application of Single Turnover active chlorophyll fluorescence for phytoplankton productivity measurements. Version 1. Report, Scientific Committee on Oceanic Research (SCOR) Working Group 156. doi:10.25607/OBP-1084.

Ulloa, O., Canfield, D.E., DeLong, E.F., Letelier, R.M., and Stewart, F.J. 2012. Microbial oceanography of anoxic oxygen minimum zones. Proceedings of the National Academy of

Sciences **109**(40): 15996–16003. Proceedings of the National Academy of Sciences. doi:10.1073/pnas.1205009109.

Ulloa, O., Henríquez-Castillo, C., Ramírez-Flandes, S., Plominsky, A.M., Murillo, A.A., Morgan-Lang, C., Hallam, S.J., and Stepanauskas, R. 2021. The cyanobacterium Prochlorococcus has divergent light-harvesting antennae and may have evolved in a low-oxygen ocean. Proceedings of the National Academy of Sciences **118**(11): e2025638118. Proceedings of the National Academy of Sciences. doi:10.1073/pnas.2025638118.

Wickham, H. 2016. Data Analysis. *In* Ggplot2: Elegant Graphics for Data Analysis. *Edited by* H. Wickham. Springer International Publishing, Cham. pp. 189–201. doi:10.1007/978-3-319-24277-4_9.

Wilson, A., Ajlani, G., Verbavatz, J.-M., Vass, I., Kerfeld, C.A., and Kirilovsky, D. 2006. A Soluble Carotenoid Protein Involved in Phycobilisome-Related Energy Dissipation in Cyanobacteria. The Plant Cell **18**(4): 992–1007. doi:10.1105/tpc.105.040121.

Wlodkowic, D., Czerw, A., Karakiewicz, B., and Deptała, A. 2022. Recent progress in cytometric technologies and their applications in ecotoxicology and environmental risk assessment. Cytometry Part A **101**(3): 203–219. doi:10.1002/cyto.a.24508.

Wong, J.C.Y., Raven, J.A., Aldunate, M., Silva, S., Gaitán-Espitia, J.D., Vargas, C.A., Ulloa, O., and von Dassow, P. 2023. Do phytoplankton require oxygen to survive? A hypothesis and model synthesis from oxygen minimum zones. Limnology and Oceanography **68**(7): 1417–1437. doi:10.1002/lno.12367.

Xu, K., Grant-Burt, J.L., Donaher, N., and Campbell, D.A. 2017. Connectivity among Photosystem II centers in phytoplankters: Patterns and responses. Biochimica et Biophysica Acta (BBA) - Bioenergetics **1858**(6): 459–474. doi:10.1016/j.bbabio.2017.03.003.

Xu, K., Lavaud, J., Perkins, R., Austen, E., Bonnanfant, M., and Campbell, D.A. 2018. Phytoplankton σPSII and excitation dissipation; implications for estimates of primary productivity. Frontiers in Marine Science **5**. doi:10.3389/fmars.2018.00281.

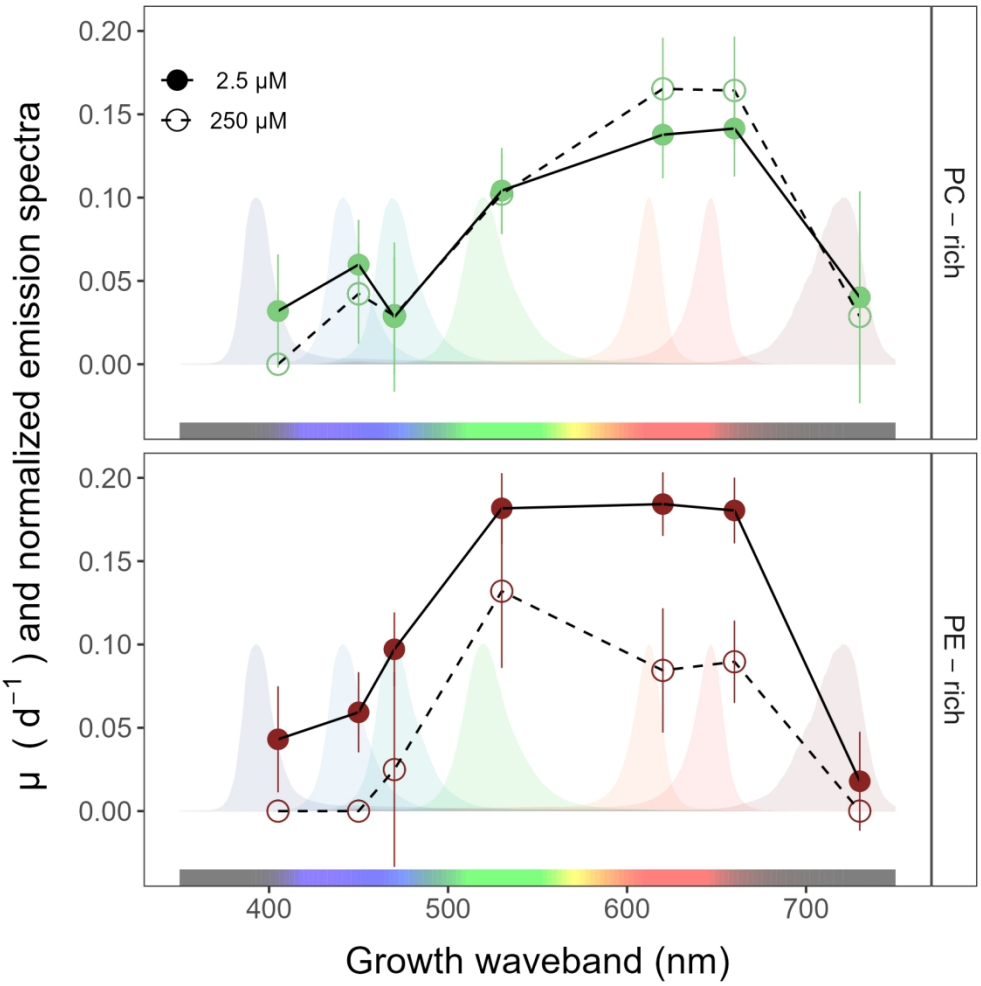

387x387mm (118 x 118 DPI)

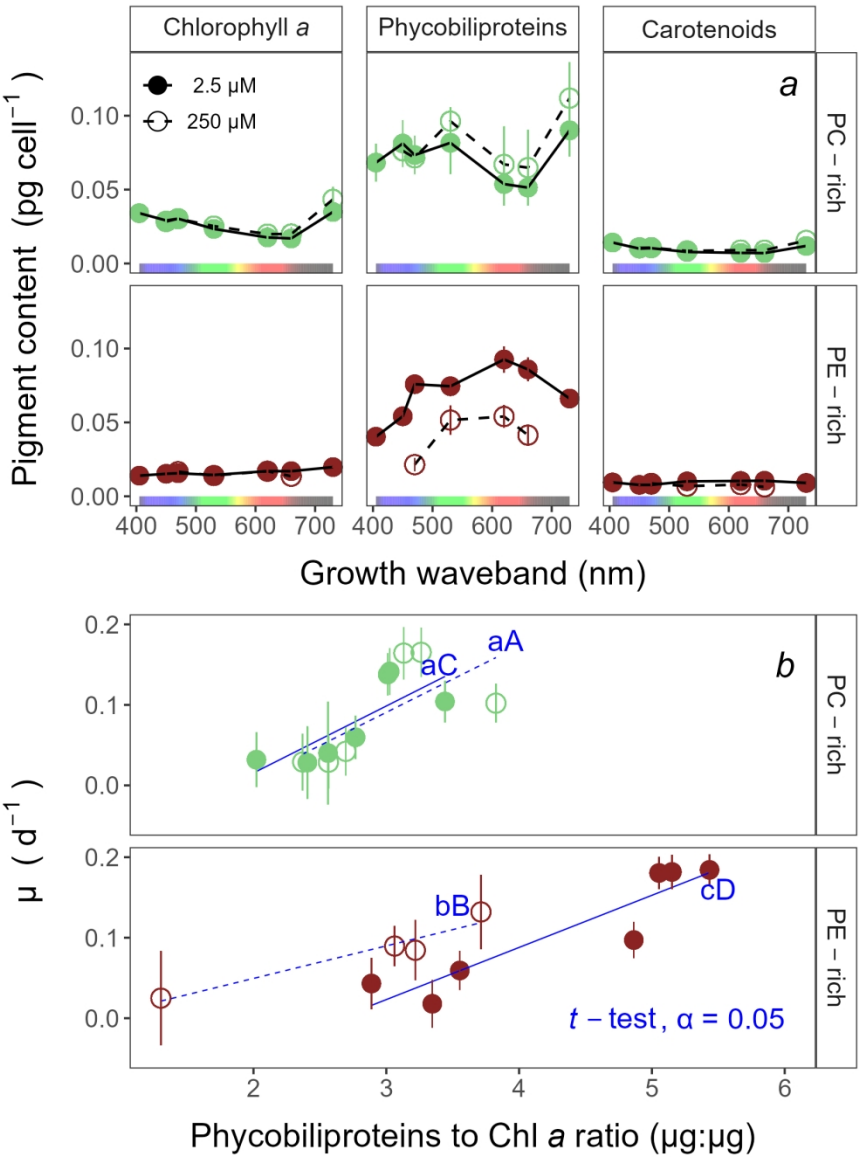

387x516mm (118 x 118 DPI)

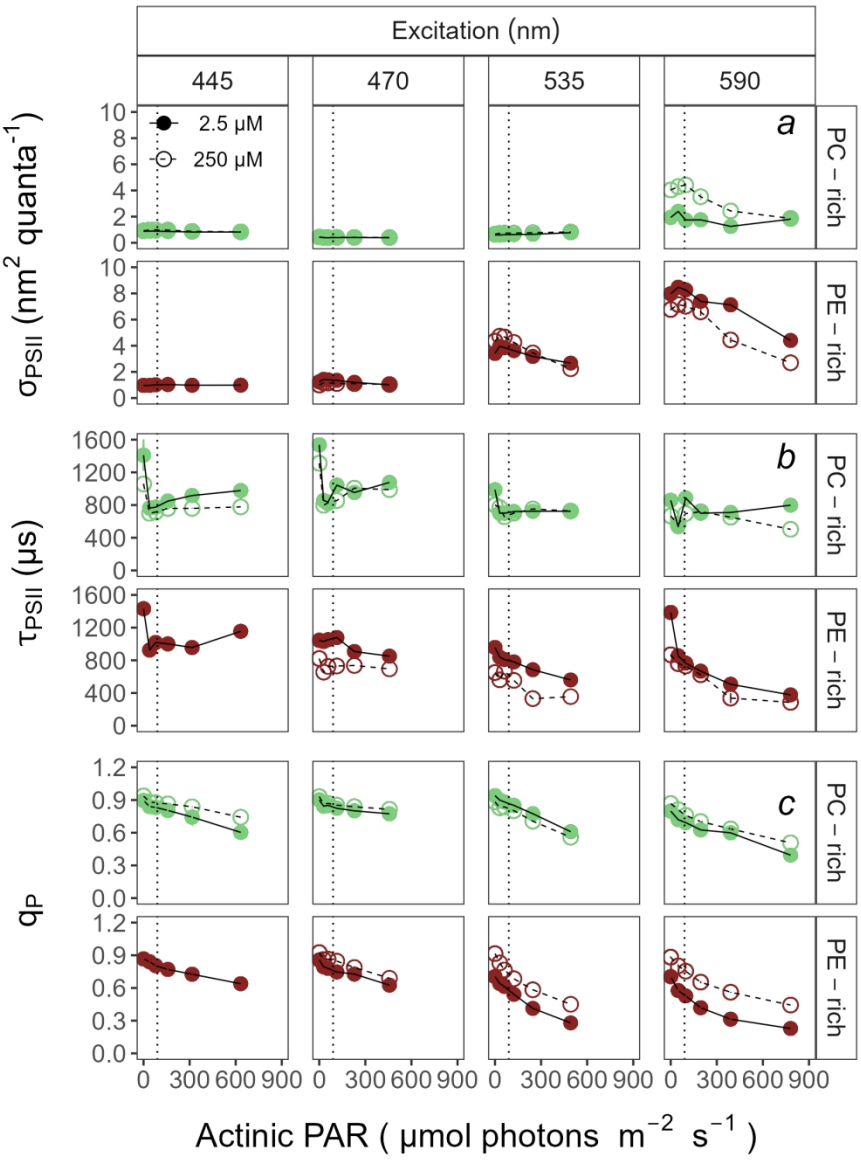

387x516mm (118 x 118 DPI)

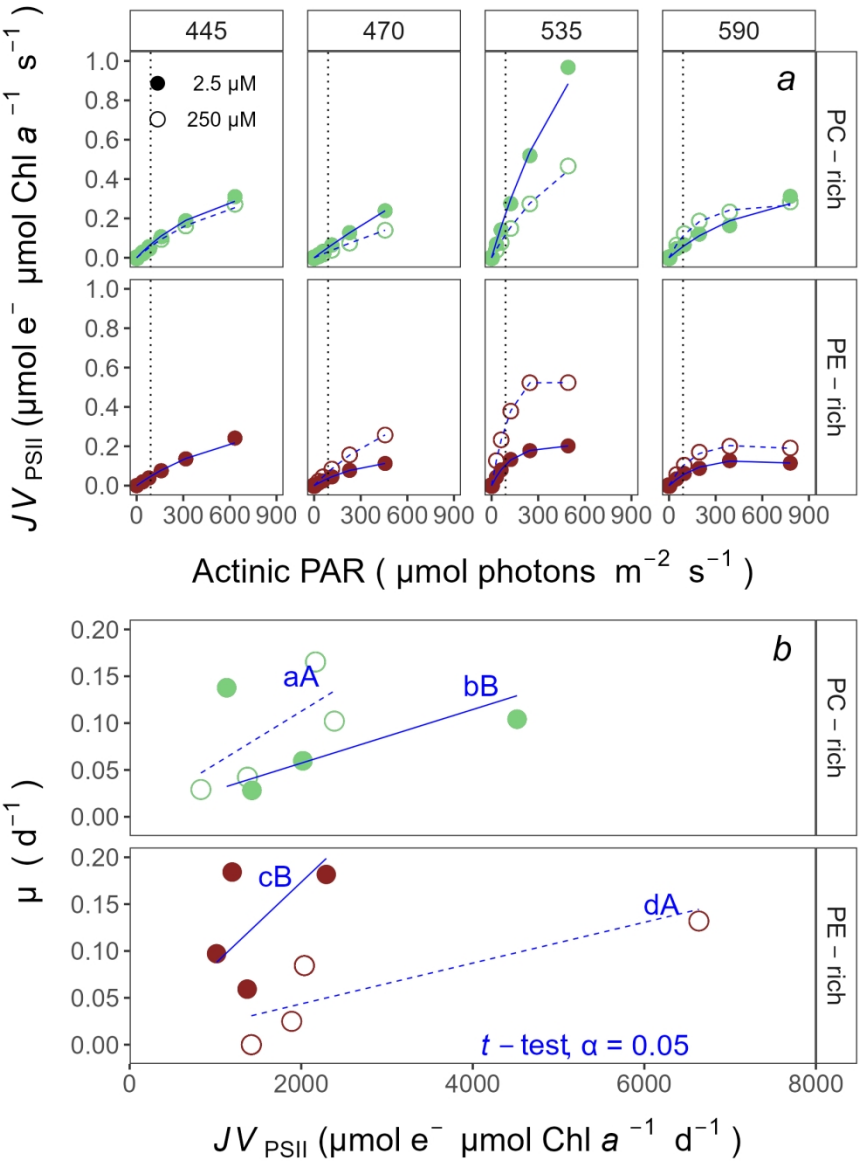

387x516mm (118 x 118 DPI)